Excited-State Electron Transfer from Ruthenium-Polypyridyl Compounds to Anatase TiO_2 Nanocrystallites: Evidence for a Stark Effect†

Shane Ardo,‡ Yali Sun,§ Felix N. Castellano,§ and Gerald J. Meyer*,‡

Departments of Chemistry and Materials Science and Engineering, Johns Hopkins University, 3400 North Charles Street, Baltimore, Maryland 21218, and Department of Chemistry and Center for Photochemical Sciences, Bowling Green State University, Bowling Green, Ohio 43403

Received: March 15, 2010; Revised Manuscript Received: May 24, 2010

Photophysical studies were performed with $[Ru(dtb)_2(dcb)](PF_6)_2$ and *cis*-$Ru(dcb)(dnb)(NCS)_2$, where dtb is 4,4′-$(C(CH_3)_3)_2$-2,2′-bipyridine, dcb is 4,4′-$(COOH)_2$-2,2′-bipyridine, and dnb is 4,4′-$(CH_3(CH_2)_8)_2$-2,2′-bipyridine), anchored to anatase TiO_2 particles (∼15 nm in diameter) interconnected in a mesoporous, thin film (∼10 μm thick) immersed in Li^+-containing acetonitrile electrolytes. Pulsed-laser excitation resulted in rapid, nonquantitative excited-state injection into TiO_2 with a rate constant that could not be time-resolved, $k_{inj} > 10^8$ s^{-1}, to yield an interfacial charge-separated state. Return of this state to ground-state products displayed observation-wavelength-dependent kinetics due to charge recombination and a second process. The second process occurred in parallel and was assigned to a transient Stark effect created by the electric field originating from the electrons in TiO_2 on ruthenium sensitizers that had not undergone excited-state injection. The kinetics for this processes were well modeled by a stretched exponential function. The impact of this field on the metal-to-ligand charge transfer excited-state of $Ru(dtb)_2(dcb)^{2+}$ or the oxidized form of *cis*-$Ru(dcb)(dnb)(NCS)_2$ were also investigated. Unambiguous identification of a Stark effect on the excited-state sensitizers was accomplished through fluence-dependent measurements. The possible influence of the electric field on the oxidized sensitizers was at best speculative. The unique relative orientation of the electric field and sensitizer afforded by the nanocrystal geometry resulted in unidirectional shifts in the absorption and photoluminescence spectra of the Ru(II) coordination compounds. On the basis of the magnitude of the shift, it was estimated that a transient field as large as 2.7 MV/cm was generated upon excited-state injection of electrons in TiO_2 at concentrations relevant to an operational dye-sensitized solar cell.

Photoinduced charge transfer in donor−acceptor assemblies results in the generation of a significant electric field. Such fields have been used to rationalize the directionality of electron flow after light absorption by the photosynthetic special pair.[1] Wasielewski and co-workers first estimated the magnitude of the field present in synthetic donor−acceptor compounds in low permittivity solutions. In what are now classical experiments, photoinduced charge separation within a porphyrin-pyromellitimide pair induced a large electrochromic shift (− 630 cm^{-1}) of a covalently bound and proximate carotenoid.[2] The shift was consistent with a ∼5.5 MV/cm electric field comparable in magnitude to those generated in natural photosynthetic systems. For fundamental studies, this observation indicated that electric fields even larger than those obtained by traditional electroabsorption (Stark) spectroscopy could be generated locally on picosecond time scales. Moreover, these workers later showed that the electric field generated by a single charge-transfer event resulted in a nearly 10-fold increase in the charge-recombination rate constant of a second charge-separated pair[3] and completely inhibited initial charge separation in another similar donor−acceptor assembly.[4] The ability to control electron-transfer rate constants with light through local electric fields has clear implications for the molecular-level design of electronic devices.[3,4]

The influence electric fields have on charge separation also has obvious relevance to solar energy conversion such as the generation of chemical fuels from sunlight. Charge-separated states have been realized that are thermodynamically capable of splitting water into hydrogen and oxygen gases.[5−7] Furthermore, recombination has been inhibited to the point that the charge-separated states are sufficiently long-lived to undergo secondary electron-transfer reactions with species in solution.[8] However, practical water splitting requires that multiple charges be transferred to and from water. This requirement presents a significant challenge as light absorption followed by electron transfer yields a single reducing equivalent and a single oxidizing equivalent in the charge-separated state while water splitting requires many. The accumulation of multiple charge-separated states through sequential absorption of multiple photons has been met with limited success due to unwanted excited-state quenching reactions. Wasielewski's finding that the electric field generated after a single charge-transfer event has a considerable impact on the electronic states of the surrounding molecules provided some new insights into the quenching mechanisms.[3,4] Practically useful molecular assemblies that integrate light absorption, charge separation, and multiple charge-transfer catalysis for solar fuel generation remain unknown, yet represent an active area of research.[9−16]

The sensitized nanocrystalline semiconductor thin films developed by Grätzel and co-workers for application in regenerative dye-sensitized solar cells (DSSCs)[17,18] have also been utilized for solar water splitting.[19−21] These mesoporous thin

† Part of the "Michael R. Wasielewski Festschrift".

* To whom correspondence should be addressed. E-mail: meyer@jhu.edu.
‡ Johns Hopkins University.
§ Bowling Green State University.

10.1021/jp102349m
Published on Web 06/21/2010

films (~10 μm thick) are comprised of interconnected anatase TiO_2 nanocrystallites (~20 nm in diameter) typically functionalized with ruthenium-polypyridyl compounds.[22] When utilized in DSSCs, the Ru(II) coordination compounds rapidly and quantitatively undergo three consecutive charge-transfer reactions: (1) light absorption through metal-to-ligand charge transfer (MLCT) excitation; (2) excited-state electron injection into TiO_2; and (3) reduction through oxidation of an electron donor present in the solution electrolyte.[22] In principle, immediately after completion of this cycle the sensitizer is "regenerated" and could repeat the "sensitization cycle" of light absorption, excited-state injection, and donor oxidation. While irradiated with 1 sun of air mass 1.5 sunlight, each sensitizer repeats this cycle on average about twice per second.[23] At the condition of maximum power generation, approximately 10 injected electrons have been estimated to reside in each TiO_2 nanocrystallite.[24] The following question arises: Do the injected electrons have a significant impact on the electronic states of the ruthenium compounds anchored to the surface?

Until recently, all experimental evidence suggested that the answer to this question was no. The high permittivity of TiO_2[25] and the half molar electrolyte commonly used in DSSCs were thought to screen the sensitizer from the field generated by the injected electrons.[17,26−41] However, recent nanosecond transient-absorption measurements after relatively intense pulsed-laser excitation showed that, after the sensitization cycle was complete, the electronic absorption spectrum of the Ru(II) sensitizers was perturbed in a manner consistent with an underlying Stark effect.[42] Very similar absorption changes could be induced with removal of small cations from the solution electrolyte or forward bias of the electrode that resulted in the electrochemical reduction of the TiO_2 nanocrystallites. The absorption shifts due to Li^+ removal were consistent with a field of magnitude 2.7 MV/cm. When the organic donor phenothiazine was used to regenerate the sensitizer, the field decayed on the same time scale as charge recombination. With iodide as the donor, a novel screening process was observed that decreased the field experienced by the Ru(II) compounds without concomitant charge recombination.[42,43]

The Stark effect was most clearly observed after the sensitization cycle was complete. However, it was suggested that the electric field was generated immediately after excited-state injection, and some preliminary data indicated that this was the case.[42] Here we report more detailed studies of the interfacial charge-separated states in the *absence* of external electron donors. The goals of this study were to better quantify the impact injected electrons have on sensitizers anchored to TiO_2. Specifically, attempts to identify transient electric-field effects in the ground state Ru(II), excited-state Ru(II)*, and oxidized Ru(III) sensitizers were explored (Scheme 1). The sensitivity of photoluminescence (PL) spectroscopy greatly aided in unambiguous identification of Stark effects in the MLCT excited state of sensitizers that had not undergone electron injection into TiO_2. Experiments were performed with dicationic Ru(II) tris-diimine and neutral Ru(II) bis-diimine bis-isothiocyanato compounds anchored to mesoporous, nanocrystalline (anatase) TiO_2 thin films that were immersed in acetonitrile electrolytes.

SCHEME 1: Photo-Induced $TiO_2(e^-)$ Formation and Subsequent Spectroscopy Employed to Monitor Stark Effects on Sensitizer Excited or Oxidized States[a]

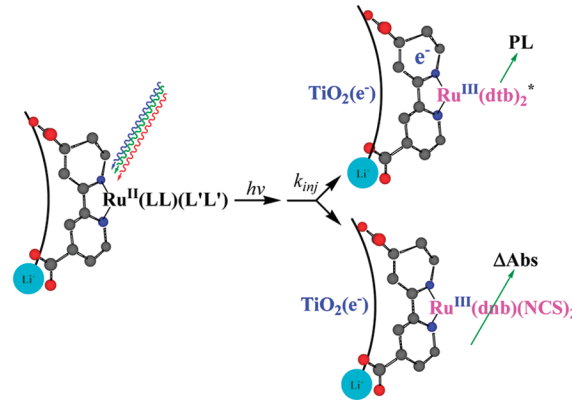

[a] Pulsed-light excitation of a TiO_2 thin film sensitized with either $[Ru^{II}(dtb)_2(dcb)]^{2+}$ or *cis*-$Ru^{II}(dcb)(dnb)(NCS)_2$ resulted in rapid excited-state electron injection (< 10 ns). The non-quantitative injection yield and rather long-lived excited state (μs) formed with Ru(II) tris-diimine compounds enabled use of time-resolved PL to monitor transiently formed Stark effects on excited states (top path). For Ru(II) bis-diimine bis-isothiocyanato compounds, efficient electron injection and long-wavelength absorption features in the Ru^{III} state enabled implementation of transient-absorption spectroscopy to investigate possible Stark effects on oxidized sensitizers (bottom path).

Experimental Section

Materials. All chemicals were reagent grade or better unless otherwise specified and were used without further purification. The following reagents and substrates were used as received from the indicated commercial suppliers: acetonitrile (Burdick & Jackson, spectrophotometric grade); lithium perchlorate (Aldrich, 99.99%); *n*-tetrabutylammonium perchlorate (TBA-ClO_4; Fluka, > 99.9%); argon gas (Airgas, > 99.998%); oxygen gas (Airgas, industrial grade); titanium(IV) isopropoxide (Sigma-Aldrich, 97%); fluorine-doped SnO_2-coated glass (FTO; Hartford Glass Co., Inc., 2.3 mm thick, 15 Ω/□); microscope slides (Fisher Scientific, 1 mm thick).

Preparations. The sensitizers employed were available from previous studies: $[Ru(dtb)_2(dcb)](PF_6)_2$ and *cis*-$Ru(dcb)(dnb)(NCS)_2$.[42]

Sensitized Metal-Oxide Thin Film. Transparent TiO_2 nanocrystallites (anatase, ~15 nm in diameter) were prepared by hydrolysis of $Ti(i\text{-}OPr)_4$ precursor using a sol−gel technique previously described in the literature.[44] The sols were cast as mesoporous thin films (~10 μm thick) by doctor blading onto glass microscope slides for spectroscopic measurements and onto transparent FTO conductive substrates for electrochemical measurements. Scotch tape was employed as a spacer. In all cases, the thin films were annealed at 420 °C for 30 min under O_2 flow.

Sensitization was achieved by immersing the supported thin films in sensitizer solutions (mM concentrations) for hours to days depending on the desired surface coverage and the rate at which the particular sensitizer reacted with the surface. Films were then soaked in the neat solvent that was used for the sensitizer binding for 5−10 min followed by a thorough washing with the experimental solvent. The samples were then quickly transferred to a standard 1 cm square quartz cuvette containing the experimental solution and were positioned diagonally (for microscope slide-supported films) or parallel (for FTO-supported films) in the cuvette. For transient absorption and electrochemical studies, the cuvettes containing the sample and electrolyte solution were purged with Ar gas for at least 30 min prior to experimentation, premoistened with the same electrolyte solution.

Spectroscopy. ***UV−Visible Absorption.*** Steady-state UV−visible (UV−vis) absorbance spectra were obtained on a Varian Cary 50 spectrophotometer at room temperature.

SCHEME 2: Ru(II) Sensitizers Employed in this Work and Their Abbreviations

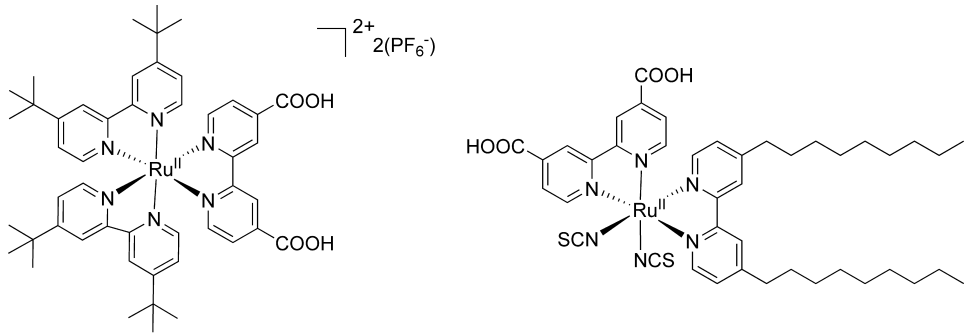

$[Ru(dtb)_2(dcb)](PF_6)_2$ *cis*-$Ru(dcb)(dnb)(NCS)_2$ (Z907)

Nanosecond transient absorption and time-resolved PL measurements were obtained with an apparatus similar to that which has been previously described.[45] Briefly, samples were excited by a pulsed Nd:YAG laser (Quantel USA (BigSky) Brilliant B; 5−6 ns full width at half-maximum (fwhm), 1 Hz, ∼10 mm in diameter) tuned to 532 nm with the appropriate nonlinear optics. An H_2 Raman shifter (∼400 psi) was employed in order to obtain Stokes-shifted 683 nm excitation. The excitation fluence was measured by a thermopile power meter (Molectron) and was typically 2−4 mJ/cm^2 per pulse so that the absorbed fluence was typically ≤1 mJ/cm^2, unless noted otherwise. A 150 W xenon arc lamp, pulsed with 100 V, served as the probe beam (Applied Photophysics) and was aligned orthogonal to the laser excitation light. Detection was achieved with a monochromator (Spex 1702/04) optically coupled to an R928 photomultiplier tube (Hamamatsu). A polarizer positioned at the magic angle relative to the polarization of the excitation light was placed prior to the monochromator in order to remove polarization-dependent signals. Transient data was acquired on a computer-interfaced digital oscilloscope (LeCroy 9450, Dual 350 MHz) with 2.5 ns resolution terminated at 50 Ω. The overall instrument response time was ∼10 ns. Typically, 60−100 laser pulses were averaged at each observation wavelength over the range 400−830 nm, at 10 nm intervals. Full spectra were generated by averaging 2−200 points on either side of the desired time value in order to help minimize noise in the raw data.

Electrochemistry. A potentiostat (BAS model CV-50W) was employed for measurements in a standard three-electrode arrangement with a sensitized TiO_2 thin film deposited on an FTO substrate working electrode, a Pt disk (Bioanalytical Scientific Instruments, Inc.) counter electrode, and an aqueous Ag/AgCl (NaCl saturated) reference electrode (Bioanalytical Scientific Instruments, Inc.). All potentials are reported versus the normal hydrogen electrode (NHE) unless otherwise noted. The ferrocenium/ferrocene ($FeCp^{2+/+}$) half-wave potential measured in a 100 mM $TBAClO_4$ acetonitrile electrolyte was used as a standard to calibrate the reference electrode, $E_{1/2}(FeCp^{2+/+}) = +531.6$ mV vs Ag/AgCl (NaCl saturated). Conversion to versus NHE was achieved using the published values for the reference electrode, i.e., + 197 mV vs NHE,[46] and correcting for the expected $E_{1/2}(FeCp^{2+/+})$ of +310 mV vs the KCl-saturated aqueous calomel electrode (SCE), where SCE is +241.2 mV vs NHE.[46] Spectroelectrochemistry was performed via application of a potential bias concurrent with monitoring the UV−vis absorbance spectra of sensitized TiO_2 thin-film electrodes.

Data Fitting. Kinetic data fitting and spectral modeling was performed in Origin 7.0 and least-squares error minimization was accomplished using the Levenberg−Marquardt iteration method. For the spectral modeling, a method for the standard addition of known spectra was developed using the C programming language and was implemented in Origin's error minimization routine.

Results

Two sensitizers were utilized for these studies, $[Ru(dtb)_2(dcb)](PF_6)_2$ and Z907 (Scheme 2). Unless noted otherwise, all experiments were performed with the sensitized thin films immersed in argon-saturated acetonitrile solutions at near maximum surface coverages.

Figure 1A shows the absorption spectra of $[Ru(dtb)_2(dcb)](PF_6)_2$ anchored to a mesoporous, nanocrystalline (anatase) TiO_2 thin film, abbreviated $Ru(dtb)_2(dcb)/TiO_2$, immersed in 100 mM $LiClO_4$ acetonitrile electrolyte or in neat acetonitrile. In the presence of Li^+, the absorption maximum red-shifted and intensity decreased relative to neat acetonitrile. Continued cycling via addition and dilution of the $LiClO_4$ electrolyte until the changes maintained nearly isosbestic points, at 433 and 486 nm ±1 nm, was performed. The corresponding data for Z907/TiO_2 are shown in Figure 1B, where the postcycling isosbestic points were approximately 406, 504, and 540.5 nm.

Transient absorption spectra recorded at the indicated delay times after pulsed-laser excitation of these sensitized thin films immersed in $LiClO_4$ acetonitrile solutions are shown in the insets of Figure 2. Inspection of the data in the insets shows that the relative shapes of the spectra are changing with time. Normalization of the long-time spectrum, which still possessed sufficient signal-to-noise, to the earliest time spectrum at a Li^+-induced Stark effect isosbestic point highlighted this fact (Figure 2). The differences of these spectra were clearly due to a similar effect observed in Figure 1, and overlaid in Figure 2 are scaled versions of the Li^+-induced difference spectra.

Wavelength-dependent kinetics were clearly observed by comparison of absorption changes monitored at a Li^+-induced Stark effect absorption minimum and isosbestic point (Figure 3). The absorption changes at this Li^+-induced Stark effect isosbestic point were used to model the charge recombination process. Under the assumption that little-to-no electric-field effects were present at longer observation times, these charge recombination data were subtracted from the absorption changes at the Stark effect minimum to obtain the absorption changes due solely to the Stark effect (Figure 3 in brown). This manipulation was performed for various wavelengths and is shown as insets in Figure 3; no clear wavelength-dependent kinetics were apparent from the insets. When normalized and compared on a logarithmic time scale, the kinetic data for the transient Stark effect for $Ru(dtb)_2(dcb)/TiO_2$ and $Z907/TiO_2$ thin

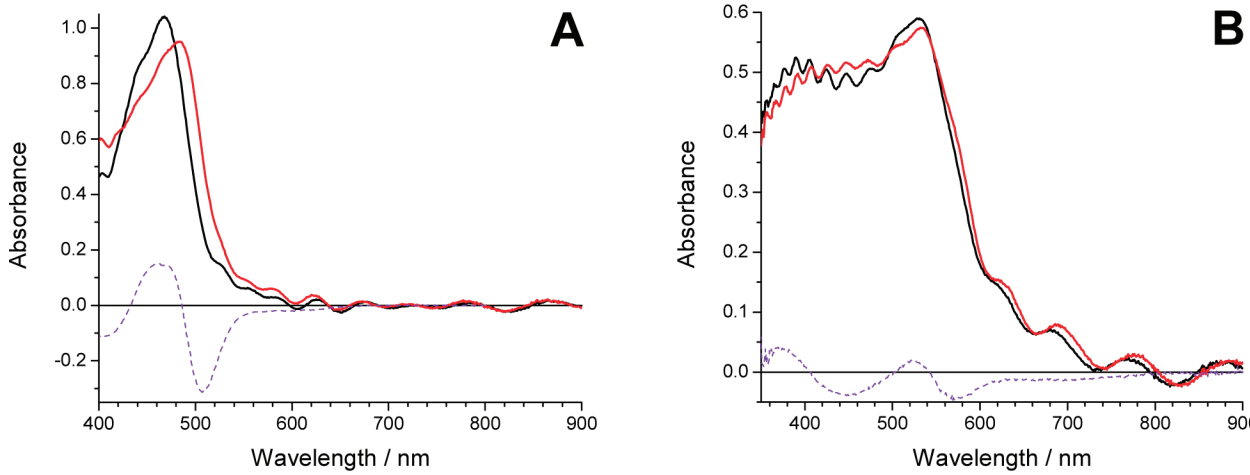

Figure 1. (A) Absorption spectra of $[Ru(dtb)_2(dcb)]^{2+}$ anchored to a TiO_2 thin film immersed in neat acetonitrile (black), 100 mM $LiClO_4/CH_3CN$ (red), and scaled difference spectrum after extensive washing (purple dashed). (B) The same spectra as in panel A but for Z907 anchored to a TiO_2 thin film. The sinusoidal shape underlying the absorption spectra is an interference pattern caused by the differing refractive indices of the thin film, electrolyte solution, and glass-slide support.

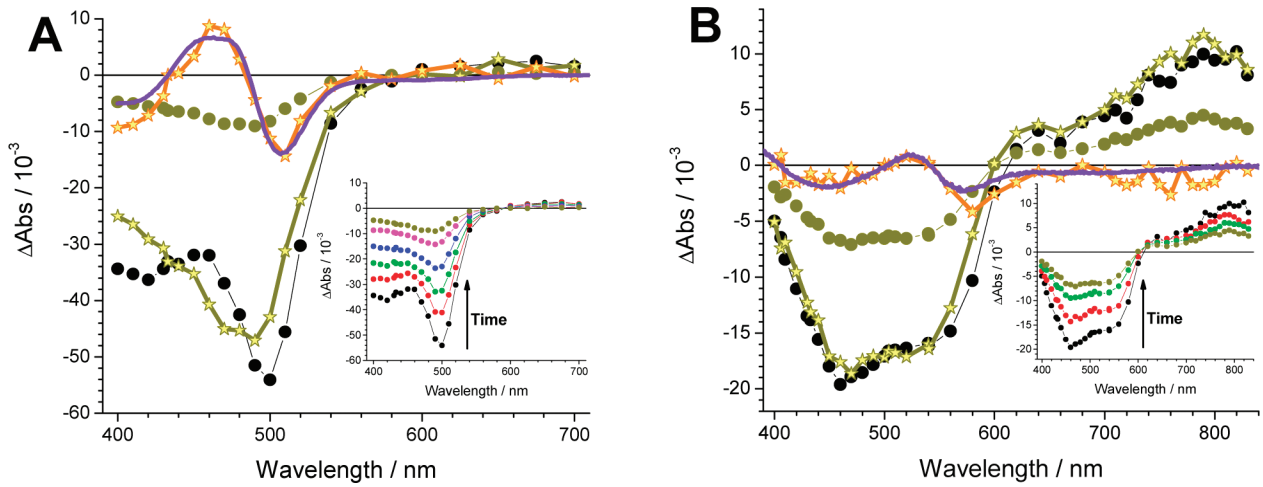

Figure 2. Transient absorption difference changes (Δ_{Abs}) and their differences ($\Delta\Delta_{Abs}$). (A) Absorption difference spectra for the $Ru(dtb)_2(dcb)/TiO_2$ thin film from Figure 1A immersed in Ar-purged 100 mM $LiClO_4/CH_3CN$ after 532 nm pulsed-laser excitation measured at 25 ns (black circles), 88 μs (brown circles), 88 μs normalized to the 25 ns spectrum at 433 nm (brown stars), and the difference spectrum between the 25 ns and scaled 88 μs spectra (orange stars). Overlaid on the latter spectrum is the scaled Li^+-induced Stark effect difference spectrum (purple) from Figure 1A. Inset: The absorption difference spectra measured at 25 ns, 200 ns, 1 μs, 5 μs, 30 μs, and 88 μs delay times. (B) Absorption difference spectra for the $Z907/TiO_2$ thin film from Figure 1B immersed in Ar-purged 100 mM $LiClO_4/CH_3CN$ after 683 nm pulsed-laser excitation measured at 25 ns (black circles), 3 μs (brown circles), 3 μs normalized to the 25 ns spectrum at 504 nm (brown stars), and the difference spectrum between the 25 ns and 3 μs spectra (orange stars). Overlaid on the latter spectrum is the scaled Li^+-induced Stark effect difference spectrum (purple) from Figure 1B. Inset: The absorption difference spectra measured at 25 ns, 200 ns, 1 μs, and 3 μs delay times.

films were practically indistinguishable, yet spanned different time domains.

The Stark effect kinetics were nonexponential but were well described by a stretched exponential function, the Kohlrausch−Williams−Watts (KWW) model[47] (eq 1):

$$I(t) = I_o \exp[-(t/\tau_o)^{\beta}] \quad (1)$$

Here β is inversely related to the width of the underlying Lévy distribution of rate constants, $0 < \beta < 1$, and τ_o is a characteristic lifetime.[48] The values obtained from best fits of the data in the insets to Figure 3 to this model along with their standard errors were $\tau_o = 3(1)$ and 0.41(4) μs and $\beta = 0.34(3)$ and 0.75(4) for $Ru(dtb)_2(dcb)/TiO_2$ and $Z907/TiO_2$, respectively. As these values were highly dependent on the long-time value chosen to normalize the kinetics, the extracted parameters should be viewed with caution. For this kinetic analysis, a long-time value was chosen such that the signal-to-noise ratio at the maximum Stark effect bleach remained greater than 5.

Figure 4A depicts the normalized, integrated time-resolved PL spectra for a $Ru(dtb)_2(dcb)/TiO_2$ thin film immersed in Ar-saturated 100 mM $LiClO_4$ acetonitrile electrolyte at the indicated laser fluences. The PL spectra generated at any time delay were practically superimposable when normalized and overlaid. The integration was performed through 1 μs, as by this time >99% of the initial signal had decayed for all fluences employed. The blue-shift in the PL spectra with increased laser fluence is indicative of a Stark effect due to the increased $TiO_2(e^-)$ concentration that resulted from the larger number of photons absorbed and hence excited-state electron-injection events. Control experiments performed on wide bandgap ZrO_2 thin films exhibited nearly zero spectral shifts (Figure S1, Supporting Information). The difference spectra shown as bold solid lines were overlaid by (a) the scaled first-derivative of the original

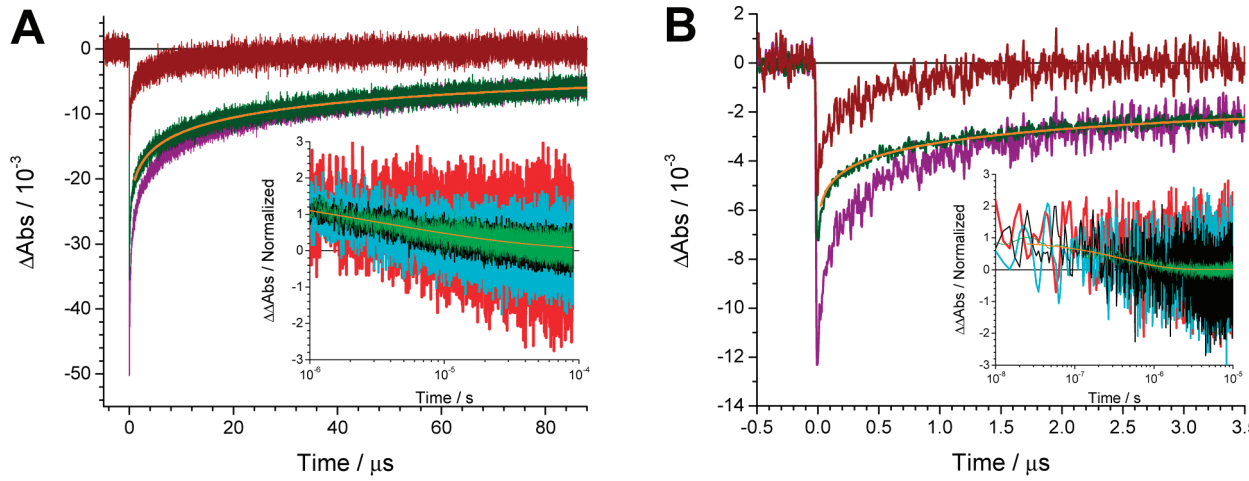

Figure 3. Transient absorption difference changes (Δ_{Abs}) and their differences ($\Delta\Delta_{Abs}$) used to generate the spectra in Figure 2 overlaid with kinetic fits to the KWW model (orange) to the data shown in green. (A) The kinetics for charge recombination from the $Ru^{III}(dtb)_2(dcb)/TiO_2(e^-)$ thin film from Figure 1A immersed in Ar-purged 100 mM $LiClO_4/CH_3CN$ were monitored at a Stark effect minimum (510 nm; purple) and isosbestic point (433 nm; green). The data at 433 nm was normalized at long times (88 μs) and subtracted to yield solely the Stark effect kinetics at 510 nm (brown). Inset: The same analysis was performed at various wavelengths where large Stark-effect signals or signals due to oxidized sensitizers would be present: 675, 460, 510, and 400 nm (back to front). **(B)** The kinetics for charge recombination for the $Z907^+/TiO_2(e^-)$ thin film from Figure 1B immersed in Ar-purged 100 mM $LiClO_4/CH_3CN$ were monitored at a Stark effect minimum (580 nm; purple) and isosbestic point (504 nm; green). The data at 504 nm was normalized at long times (3 μs) and subtracted to yield solely the Stark effect kinetics at 580 nm (brown). Inset: The same analysis was performed at various wavelengths where large Stark-effect signals or signals due to oxidized sensitizers would be present: 520, 800, 450, and 580 nm (back to front).

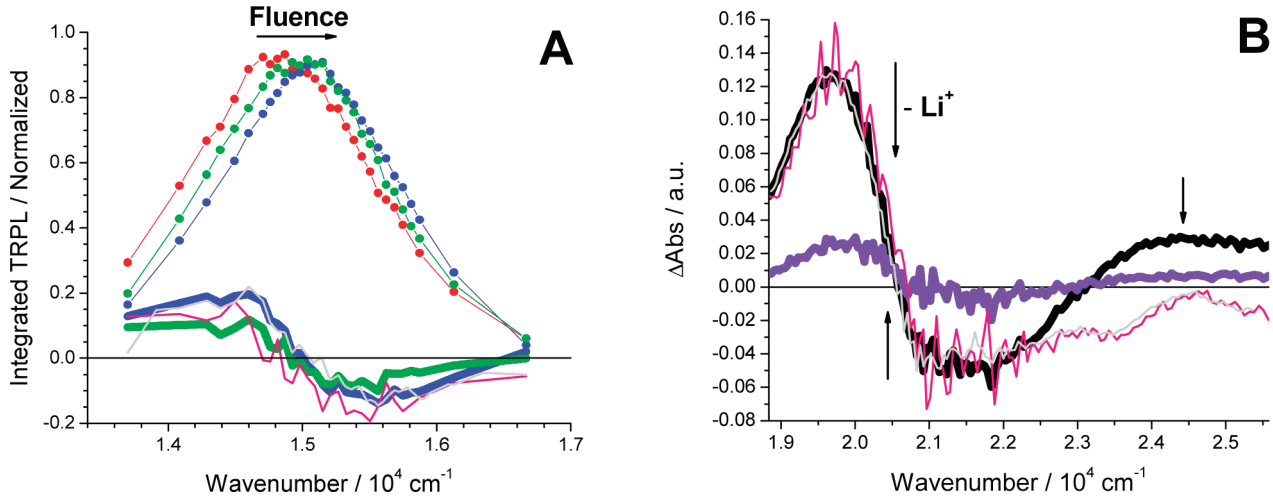

Figure 4. (A) Integrated time-resolved PL spectra for a $Ru(dtb)_2(dcb)/TiO_2$ thin film immersed in Ar-purged 100 mM $LiClO_4/CH_3CN$ at pulse fluences in mJ/cm^2 of 0.025 (red), 0.45 (green), and 2.7 (blue). Also shown are the difference spectra with the same color scheme (bold lines) between the lowest fluence and the others. Overlaid on the blue difference spectrum are spectral simulations using scaled versions of (a) the first-derivative of the lowest fluence spectrum (pink) and (b) the difference between the lowest fluence spectrum and the same spectrum shifted 215 cm^{-1} (gray). (B) Difference absorption spectra for a $Ru(dtb)_2(dcb)/TiO_2$ thin film immersed in 500 mM $LiClO_4/CH_3CN$ (black) and after a series of 1:2, v/v dilution to 2 mM (purple) all referenced to the spectrum at 0.49 mM $LiClO_4$. Overlaid on the 500 mM difference spectrum are spectral simulations using scaled versions of (a) the first-derivative of the original lowest [$LiClO_4$] spectrum (pink) and (b) the difference between the original lowest [$LiClO_4$] spectrum and the same spectrum shifted 220 cm^{-1} (gray).

spectrum at low fluence and (b) the difference in a scaled and 215 cm^{-1} shifted version of the original spectrum also at low fluence.

Figure 4B shows the difference absorption spectra (bold solid lines) for a $Ru(dtb)_2(dcb)/TiO_2$ thin film immersed in acetonitrile electrolyte at various concentrations of $LiClO_4$. Overlaid are the scaled (a) first-derivative of the original absorption spectrum at low [$LiClO_4$] and (b) difference in a 220 cm^{-1} shifted version of the original spectrum at low [$LiClO_4$].

In the absence of a significant change in polarizability between the ground and excited state, the magnitude of the electric field experienced by the ruthenium-polypyridyl compounds was calculated via eq 2:[2,49,50]

$$\Delta\bar{\nu} = -\frac{|\Delta\vec{\mu}| \cdot |\vec{E}| \cdot \cos\theta}{100hc} \quad (2)$$

where h is Planck's constant, c is the speed of light in a vacuum, $\Delta\bar{\nu}$ is the change in the spectroscopic peak maximum (in wavenumbers), $\Delta\vec{\mu}$ is the change in dipole moment vector between the ground and excited state, $\vec{E}$ is the electric field vector, and θ is the angle between the latter two. Both the maximum fluence-induced PL shift and Li^+-induced absorption shift were ~215 cm^{-1}. Oh and Boxer calculated a $|\Delta\vec{\mu}| \approx 4.75$ D for the lowest energy ^{1}MLCT transition of a related heteroleptic Ru(II)-polypyridyl compound.[51] Assuming the dipole moments for the ground and photoluminescent excited

(thexi) state are both oriented antiparallel with respect to the electric field emanating from the TiO_2 surface, and thus $\theta = 180$, an electric field intensity of ~2.7 MV/cm is obtained.[2,52]

Discussion

Evidence for Stark effects at sensitized metal-oxide semiconductor interfaces is apparent in previously published data based on spectroelectrochemistry,[42,53] transient-absorption spectroscopy,[42,43,54,55] and Li^+ induced shifts in the visible absorption spectrum.[42,43,56] The results presented herein indicate that Stark effects are present immediately upon excited-state electron injection and affect not only sensitizers in their Ru(II) ground states but also those in their thermally equilibrated MLCT excited states. Therefore, like molecular charge separation in the aforementioned artificial and natural photosynthetic donor−acceptor assemblies,[1−4] a substantial electric field is photogenerated at sensitized semiconductor interfaces. Below we discuss evidence for the generation of the transient electric field and how it influences the ground, excited, and oxidized states of the sensitizer, followed by a description of the magnitude and unique orientation of the field relative to the surface-anchored compounds.

Generation and Influence of the Electric Field. The MLCT excited states of ruthenium-polypyridyl compounds are known to inject electrons into TiO_2 on femto- to picosecond time scales in acetonitrile electrolytes.[22] Once vibrational/phonon relaxation is complete, a single charge-separated state is expected, comprised of an electron in TiO_2 and an oxidized sensitizer present in the formal oxidation state of Ru(III). In principle, this state should recombine to ground-state products with wavelength independent kinetics. However, this was not observed. Careful spectral analysis allowed for the unambiguous identification of absorption features expected for the charge-separated state *and* Ru(II) compounds in an environment different from that which was initially excited. The time scale for loss of this Stark effect indicates that it is likely due to contributions from both the loss of the transient electric field, due to interfacial charge recombination, and ionic redistribution to screen the field created by the injected electron. The kinetics for parallel charge recombination and ionic screening were well described by the stretched exponential function that was previously derived based on multiple-trapping, continuous-time random walks,[57−63] and dielectric relaxation.[47,59,64] The kinetic analysis suggests that screening was about 2 orders of magnitude more rapid for the neutral Z907 sensitizer than for the dicationic $Ru(dtb)_2(dcb)^{2+}$ compound. However, it proved difficult to cleanly separate charge recombination from the screening kinetics, as identification of a time period where the Stark effect was absent was somewhat arbitrary. Nevertheless, the data clearly showed that the Stark effect was present 10 ns after excited-state injection and with faster time resolution, we fully anticipate that the effect would be observed immediately after excited-state injection. While the kinetic rate constants for ionic screening were less certain, the <100 μs time scale identified was in good agreement with previous expectations.[43]

Judicious choice of the ruthenium-polypyridyl compounds allowed for investigation of how Stark effects influenced the oxidized and MLCT excited states of the sensitizers. The Z907/TiO_2 thin film samples were specifically chosen as $Z907^+$ possesses a new absorption band with considerable oscillator strength in the red and near-infrared regions. This transition is well-known and has previously been attributed to $NCS^- \rightarrow Ru^{III}$ ligand-to-metal charge transfer (LMCT) transitions.[65,66] The fact that wavelength-dependent kinetics were observed at $\lambda > 800$ nm for Z907/TiO_2 thin films (Figures 2B and 3B) suggested a Stark effect on $Z907^+$. Unfortunately, the effect could not be cleanly identified due to poorer sensitivity in this spectral region and the low concentration of oxidized sensitizers generated with light. The experiments were further hampered by our inability to generate an authentic reference spectrum of $Z907^+/TiO_2$ in the presence and absence of Li^+. The $Z907^+/TiO_2$ absorption spectrum was generated electrochemically in $TBAClO_4$ acetonitrile electrolyte (Figure S2, Supporting Information). Unfortunately, removal of the electrolyte via dilution induced sensitizer desorption and/or degradation. This was not surprising as ruthenium-polypyridyl compounds containing isothiocyanate ligands are known to be less stable in their oxidized forms.[67−70]

The $Ru(dtb)_2(dcb)/TiO_2$ thin film samples were specifically chosen for investigation as they exhibited a sizable Ru(II) Stark effect and have a long-lived MLCT excited state. These characteristics allowed for observation of room temperature PL from $Ru(dtb)_2(dcb)/TiO_2$, even when immersed in a 100 mM $LiClO_4$ acetonitrile electrolyte. It had been previously noted that the PL spectra of ruthenium-polypyridyl compounds anchored to TiO_2 were sensitive to the presence of $LiClO_4$.[42,43,56] Herein we have demonstrated that a blue shift can be observed by increasing the $TiO_2(e^-)$ concentration within the nanocrystallites with increased laser fluence. The PL decay did not show any wavelength dependence, and the entire spectra decayed symmetrically. This presumably occurred because the relatively short submicrosecond lifetime meant that the excited state did not experience a significant change in the $TiO_2(e^-)$ concentration. In theory, the same $TiO_2(e^-)$ concentration could be generated with a forward bias and the PL spectrum measured. Indeed, blue-shifted PL spectra were observed; however, such measurements led to irreversible chemistry that complicated analysis.

Electric Field Magnitude and Orientation. Classical Stark measurements of Ru(II)-polypyridyl compounds indicate that a large dipole moment change underlies the electroabsorption behavior with a negligible contribution due to polarizability.[51,71−78] Oh and Boxer reported a change in dipole moment of $|\Delta\vec{\mu}| \approx 4.75$ D for the lowest energy ^{1}MLCT transition of a related heteroleptic Ru(II)-polypyridyl compound.[51] With this value as an estimate of $|\Delta\vec{\mu}|$ and the ~215 cm^{-1} shift measured in the absorption and PL spectra, an electric field intensity of ~2.7 MV/cm was calculated by eq 2. It is interesting to note that the unscreened electric field present within the first microsecond after excited-state injection corresponds to <10 $TiO_2(e^-)$s/particle, a value approximately equal to that expected at the power point of an operational DSSC. This field strength is also on the order observed in proteins and for artificial donor−acceptor compounds in low permittivity solvents.[52,79−81] The field is much stronger than one would expect based on the permittivities of TiO_2 and acetonitrile. We note, however, that there is considerable experimental uncertainty in the permittivity of anatase TiO_2,[25] and that effective permittivities at interfaces are often very different than their bulk values.[1,52,80,82−87] A striking and well-known example is water electrolytes whose relative permittivity of 80 is reduced to <10 in the inner Helmholtz region of the double layer at polarized metal electrode interfaces.[85]

Electroabsorption data is often modeled by comparisons with the first, second, and even higher derivatives of the ground-state spectrum.[49,50] Significant experimental noise often requires that the derivatives be taken of noise-free simulated data. This was not the case for the data reported here. Surprisingly, the data were well modeled by the first-derivative of the original spectrum. This was *not* expected, as traditional electroabsorption analysis under the Liptay treatment predicts that a change in

SCHEME 3: Sensitized Thin-Film Geometry, Electric-Fields Lines, and Expected Spectroscopic Changes[a]

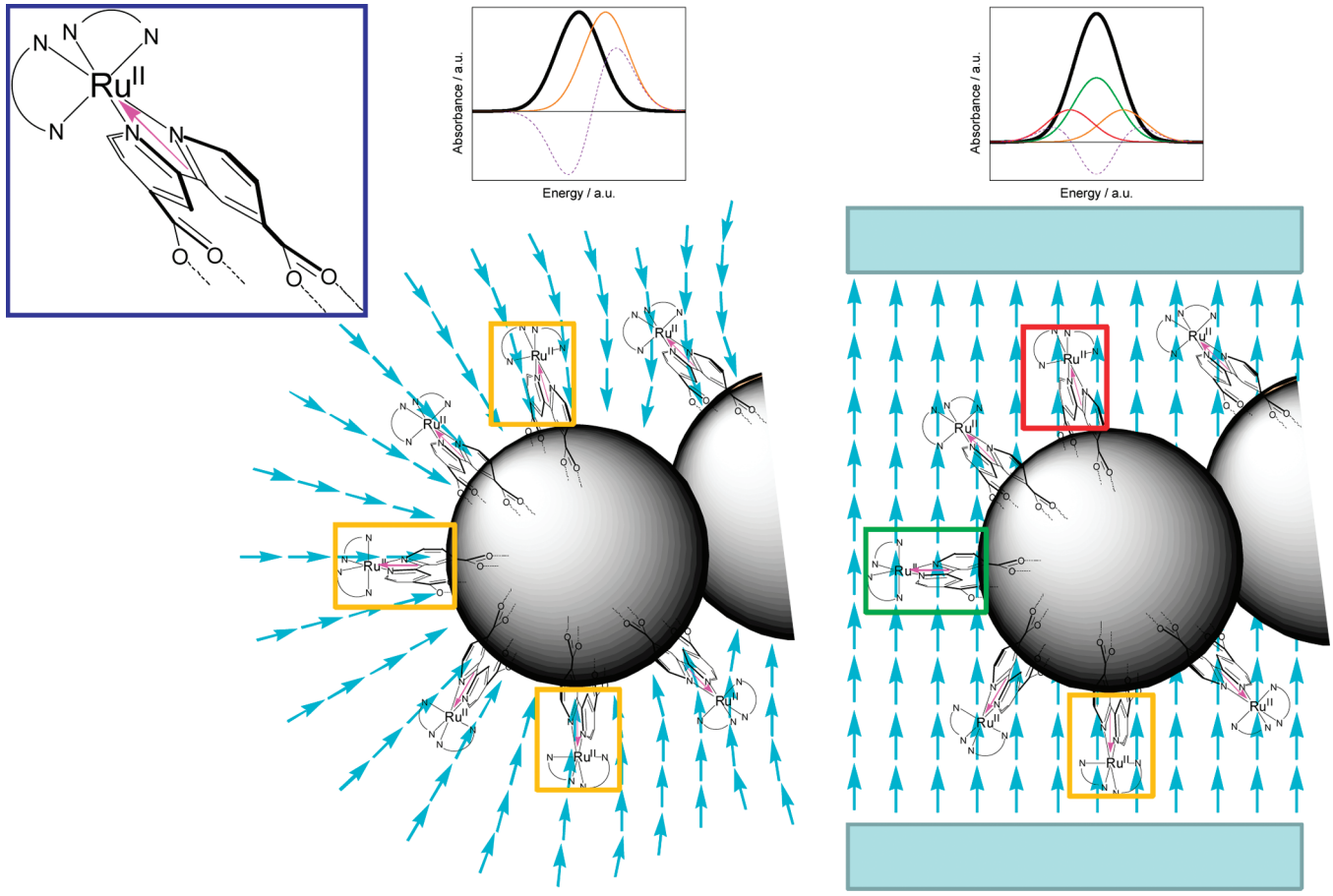

[a] Top/Left Inset: A representation of a Ru(II)-polypyridyl coordination compound with the change in dipole moment for its lowest-energy ^{1}MLCT transition shown in magenta. Middle: Vectors for the proposed electric field (cyan) generated by the charged TiO_2 nanocrystallites as part of a thin film. Right: Electric-field vectors (oversimplification as the lines should curve towards the TiO_2 when in close proximity) for the same sample if it were measured by typical electroabsorption spectroscopy in the absence of TiO_2-based electric fields. Top Inset: Simulated absorption spectra of a hypothetical thin film in the absence (black) and presence (colored) of the electric field for each scenario, along with their resulting difference spectra (purple dashed).

dipole moment, $\Delta\vec{\mu}$, would give rise to a second-derivative spectrum rather than the first-derivative observed.[49,50] We attribute this to the unique collinear alignment of the MLCT change in dipole moment and the electric field afforded by the TiO_2 nanocrystallite material as described further below.

Scheme 3 shows the electric-field vectors expected for $Ru(dtb)_2(dcb)/TiO_2$ in a classical Stark experiment between two polarized electrodes and when the electric field emanates from the TiO_2 nanocrystallites after excited-state injection. In the classical experimental arrangement, the field has an equal probability of being aligned with and against the dipole-moment change. Under the assumption of predominantly dipolar-based interactions, this would result in a spectrum that was red-shifted for some of the compounds and blue-shifted for others, which would collectively resemble a second-derivative spectrum. In fact, if the nanocrystallites were absent and the same orientation of the Ru compounds existed in an immobilized frozen solid-state medium, the spectrum would be that observed in typical electroabsorption measurements.

When the field is generated by excited-state injection, its orientation is very different. While the random overall distribution of sensitizers remains unchanged, the field orientation with respect to each sensitizer's lowest-energy change in dipole moment is always predominantly antiparallel. This would result in a unidirectional shift of the absorption spectrum, which resembles its first-derivative spectrum. Therefore, the sensitizer−TiO_2 nanocrystallite geometry should solely result in a unidirectional shift for all surface-anchored molecules.[2,49,50] Thus, effects due to either $\Delta\vec{\mu}$ or $\Delta\underline{\alpha}$ would result in spectra that resembled first-derivatives of the original spectrum.

Scheme 3 does not take into account the necking regions between TiO_2 nanocrystallites that support the mesoporous thin film or the fact that only the Ru → dcb dipole change is aligned with the field, while the Ru → dtb and Ru → dnb are not. In fact, based on this analysis, the Stark effect on the thexi state with excited electron localization on the dcb ligand, i.e., $Ru^{III}(dtb)_2(dcb^-)^*/TiO_2$, of an isolated spherical particle would strictly be expected to give rise to a first-derivative spectrum. Necking regions and additional charge-transfer transitions should complicate the observed spectra of these heteroleptic ruthenium compounds anchored to mesoporous nanocrystalline thin films. We can only suggest that the necking regions and additional charge-transfer transitions have a negligible contribution to the observed Stark behavior.

Conclusions

The experimental data provides compelling evidence that excited-state injection of electrons into TiO_2 nanocrystallites interconnected in a mesoporous thin film creates an electric field that perturbs the energetics of the MLCT absorption bands of Ru(II) compounds anchored to the same surface. This electric

field also has a significant impact on the MLCT excited state that manifests itself as a blue shift in the PL spectrum with increased $TiO_2(e^-)$ concentration. The spectral data is well modeled as a first-derivative of the steady-state spectrum, behavior that is attributed to the unique orientation of the charge-transfer change in dipole moment and the electric field. With some assumptions, the electric field created by injection of <10 electrons per nanocrystallite generates a field of ~2.7 MV/cm.

Acknowledgment. The JHU portion of the work was supported by the Division of Chemical Sciences, Office of Basic Energy Sciences, Office of Energy Research, U.S. Department of Energy (DE-FG02-96ER14662). S. A. acknowledges a Johns Hopkins University Greer graduate student fellowship. The BGSU portion of the work was supported by the National Science Foundation (CHE-0719050) and the Air Force Office of Scientific Research (FA9550-05-1-0276).

Supporting Information Available: Comparative fluence-dependent PL spectra for $[Ru(dtb)_2(dcb)]^{2+}$ anchored to either TiO_2 or ZrO_2 thin films and the $Z907^+/TiO_2$ absorption difference spectrum generated spectroelectrochemically. This material is available free of charge via the Internet at http://pubs.acs.org/.

References and Notes

(1) Steffen, M. A.; Lao, K.; Boxer, S. G. *Science* **1994**, *264*, 810–816.
(2) Gosztola, D.; Yamada, H.; Wasielewski, M. R. *J. Am. Chem. Soc.* **1995**, *117*, 2041–2048.
(3) Debreczeny, M. P.; Svec, W. A.; Wasielewski, M. R. *Science* **1996**, *274*, 584–587.
(4) Gosztola, D.; Niemczyk, M. P.; Wasielewski, M. R. *J. Am. Chem. Soc.* **1998**, *120*, 5118–5119.
(5) Juris, A.; Balzani, V.; Barigelletti, F.; Campagna, S.; Belser, P.; von Zelewsky, A. *Coord. Chem. Rev.* **1988**, *84*, 85–277.
(6) In *Organic Chemistry and Theory*; Boschke, F. L.; Dewar, M. J. S.; Harrier, K.; Heilbronner, E.; Itô, S.; Lehn, J.-M.; Neidenzu, K.; Rees, C. W.; Schäfer, K.; Wittig, G., Eds.; Topics in Current Chemistry; Springer-Verlag: Berlin, Heidelberg, New York, 1978; Vol. 75.
(7) Brown, G. M.; Brunschwig, B. S.; Creutz, C.; Endicott, J. F.; Sutin, N. *J. Am. Chem. Soc.* **1979**, *101*, 1298–1300.
(8) Meyer, T. J. *Acc. Chem. Res.* **1989**, *22*, 163–170.
(9) Morris, A. J.; Meyer, G. J.; Fujita, E. *Acc. Chem. Res.* **2009**, *42*, 1983–1994.
(10) Dempsey, J. L.; Brunschwig, B. S.; Winkler, J. R.; Gray, H. B. *Acc. Chem. Res.* **2009**, *42*, 1995–2004.
(11) Magnuson, A.; Anderlund, M.; Johansson, O.; Lindblad, P.; Lomoth, R.; Polivka, T.; Ott, S.; Stensjö, K.; Styring, S.; Sundström, V.; Hammarström, L. *Acc. Chem. Res.* **2009**, *42*, 1899–1909.
(12) Wasielewski, M. R. *Acc. Chem. Res.* **2009**, *42*, 1910–1921.
(13) Youngblood, W. J.; Lee, S.-H. A.; Maeda, K.; Mallouk, T. E. *Acc. Chem. Res.* **2009**, *42*, 1966–1973.
(14) Gust, D.; Moore, T. A.; Moore, A. L. *Acc. Chem. Res.* **2009**, *42*, 1890–1898.
(15) Concepcion, J. J.; Jurss, J. W.; Brennaman, M. K.; Hoertz, P. G.; Patrocinio, A. O. T.; Murakami Iha, N. Y.; Templeton, J. L.; Meyer, T. J. *Acc. Chem. Res.* **2009**, *42*, 1954–1965.
(16) Boettcher, S. W.; Spurgeon, J. M.; Putnam, M. C.; Warren, E. L.; Turner-Evans, D. B.; Kelzenberg, M. D.; Maiolo, J. R.; Atwater, H. A.; Lewis, N. S. *Science* **2010**, *327*, 185–187.
(17) O'Regan, B.; Moser, J.; Anderson, M.; Grätzel, M. *J. Phys. Chem.* **1990**, *94*, 8720–8726.
(18) O'Regan, B.; Grätzel, M. *Nature* **1991**, *353*, 737–740.
(19) Youngblood, W. J.; Lee, S.-H. A.; Kobayashi, Y.; Hernandez-Pagan, E. A.; Hoertz, P. G.; Moore, T. A.; Moore, A. L.; Gust, D.; Mallouk, T. E. *J. Am. Chem. Soc.* **2009**, *131*, 926–927.
(20) Li, G.; Sproviero, E. M.; Iii, R. C. S.; Iguchi, N.; Blakemore, J. D.; Crabtree, R. H.; Brudvig, G. W.; Batista, V. S. *Energy Environ. Sci.* **2009**, *2*, 230–238.
(21) Liu, F.; Cardolaccia, T.; Hornstein, B. J.; Schoonover, J. R.; Meyer, T. J. *J. Am. Chem. Soc.* **2007**, *129*, 2446–2447.
(22) Ardo, S.; Meyer, G. J. *Chem. Soc. Rev.* **2009**, *38*, 115–164.
(23) Grätzel, M. *CATTECH* **1999**, *3*, 4–17.
(24) O'Regan, B. C.; Durrant, J. R. *Acc. Chem. Res.* **2009**, *42*, 1799–1808.
(25) Olson, C. L.; Nelson, J.; Islam, M. S. *J. Phys. Chem. B* **2006**, *110*, 9995–10001.
(26) Gregg, B. A. *Coord. Chem. Rev.* **2004**, *248*, 1215–1224.
(27) Nelson, J. *Phys. Rev. B* **1999**, *59*, 15374–15380.
(28) Schlichthorl, G.; Huang, S. Y.; Sprague, J.; Frank, A. J. *J. Phys. Chem. B* **1997**, *101*, 8141–8155.
(29) Schwarzburg, K.; Willig, F. *J. Phys. Chem. B* **1999**, *103*, 5743–5746.
(30) Dloczik, L.; Ileperuma, O.; Lauermann, I.; Peter, L. M.; Ponomarev, E. A.; Redmond, G.; Shaw, N. J.; Uhlendorf, I. *J. Phys. Chem. B* **1997**, *101*, 10281–10289.
(31) Zaban, A.; Meier, A.; Gregg, B. A. *J. Phys. Chem. B* **1997**, *101*, 7985–7990.
(32) Hendry, E.; Koeberg, M.; O'Regan, B.; Bonn, M. *Nano Lett.* **2006**, *6*, 755–759.
(33) Zaban, A.; Ferrere, S.; Gregg, B. A. *J. Phys. Chem. B* **1998**, *102*, 452–460.
(34) Gregg, B. A. *J. Phys. Chem. B* **2003**, *107*, 13540–13540.
(35) Könenkamp, R. *Phys. Rev. B* **2000**, *61*, 11057–11064.
(36) Kytin, V.; Dittrich, T.; Bisquert, J.; Lebedev, E. A.; Koch, F. *Phys. Rev. B* **2003**, *68*, 195308.
(37) Hoyer, P.; Weller, H. *J. Phys. Chem.* **2002**, *99*, 14096–14100.
(38) Brus, L. *Phys. Rev. B* **1996**, *53*, 4649–4656.
(39) Cahen, D.; Hodes, G.; Grätzel, M.; Guillemoles, J. F.; Riess, I. *J. Phys. Chem. B* **2000**, *104*, 2053–2059.
(40) Bisquert, J.; Cahen, D.; Hodes, G.; Ruhle, S.; Zaban, A. *J. Phys. Chem. B* **2004**, *108*, 8106–8118.
(41) Olson, C. L. *J. Phys. Chem. B* **2006**, *110*, 9619–9626.
(42) Ardo, S.; Sun, Y.; Staniszewski, A.; Castellano, F. N.; Meyer, G. J. *J. Am. Chem. Soc.* **2010**, *132*, 6696–6709.
(43) Staniszewski, A.; Ardo, S.; Sun, Y.; Castellano, F. N.; Meyer, G. J. *J. Am. Chem. Soc.* **2008**, *130*, 11586–11587.
(44) Heimer, T. A.; D'Arcangelis, S. T.; Farzad, F.; Stipkala, J. M.; Meyer, G. J. *Inorg. Chem.* **1996**, *35*, 5319–5324.
(45) Argazzi, R.; Bignozzi, C. A.; Heimer, T. A.; Castellano, F. N.; Meyer, G. J. *Inorg. Chem.* **1994**, *33*, 5741–5749.
(46) Bard, A. J.; Faulkner, L. R. *Electrochemical Methods: Fundamentals and Applications*, 2nd ed.; John Wiley & Sons, Inc.: New York, 2001.
(47) Williams, G.; Watts, D. C. *Trans. Faraday Soc.* **1970**, *66*, 80–85.
(48) Xia, H.-L.; Ardo, S.; Narducci Sarjeant, A. A.; Huang, S.; Meyer, G. J. *Langmuir* **2009**, *25*, 13641–13652.
(49) Boxer, S. G. *J. Phys. Chem. B* **2009**, *113*, 2972–2983.
(50) Bublitz, G. U.; Boxer, S. G. *Annu. Rev. Phys. Chem.* **1997**, *48*, 213–242.
(51) Oh, D. H.; Boxer, S. G. *J. Am. Chem. Soc.* **1989**, *111*, 1130–1131.
(52) Lockhart, D. J.; Kim, P. S. *Science* **1992**, *257*, 947–951.
(53) Cappel, U. B.; Gibson, E. A.; Hagfeldt, A.; Boschloo, G. *J. Phys. Chem. C* **2009**, *113*, 6275–6281.
(54) Montanari, I.; Nelson, J.; Durrant, J. R. *J. Phys. Chem. B* **2002**, *106*, 12203–12210.
(55) Nasr, C.; Hotchandani, S.; Kamat, P. V. *J. Phys. Chem. B* **1998**, *102*, 4944–4951.
(56) Kelly, C. A.; Farzad, F.; Thompson, D. W.; Stipkala, J. M.; Meyer, G. J. *Langmuir* **1999**, *15*, 7047–7054.
(57) Scher, H.; Montroll, E. W. *Phys. Rev. B* **1975**, *12*, 2455–2477.
(58) Pfister, G.; Scher, H. *Adv. Phys.* **1978**, *27*, 747–798.
(59) Shlesinger, M. F.; Montroll, E. W. *Proc. Natl. Acad. Sci. U.S.A.* **1984**, *81*, 1280–1283.
(60) Nelson, J.; Chandler, R. E. *Coord. Chem. Rev.* **2004**, *248*, 1181–1194.
(61) Nelson, J.; Haque, S. A.; Klug, D. R.; Durrant, J. R. *Phys. Rev. B* **2001**, *63*, 205321.
(62) Katoh, R.; Furube, A.; Barzykin, A. V.; Arakawa, H.; Tachiya, M. *Coord. Chem. Rev.* **2004**, *248*, 1195–1213.
(63) Barzykin, A. V.; Tachiya, M. *J. Phys. Chem. B* **2004**, *108*, 8385–8389.
(64) Palmer, R. G.; Stein, D. L.; Abrahams, E.; Anderson, P. W. *Phys. Rev. Lett.* **1984**, *53*, 958–961.
(65) Tachibana, Y.; Moser, J. E.; Grätzel, M.; Klug, D. R.; Durrant, J. R. *J. Phys. Chem.* **1996**, *100*, 20056–20062.
(66) Das, S.; Kamat, P. V. *J. Phys. Chem. B* **1998**, *102*, 8954–8957.
(67) Nazeeruddin, M. K.; Zakeeruddin, S. M.; Lagref, J. J.; Liska, P.; Comte, P.; Barolo, C.; Viscardi, G.; Schenk, K.; Grätzel, M. *Coord. Chem. Rev.* **2004**, *248*, 1317–1328.
(68) Cecchet, F.; Gioacchini, A. M.; Marcaccio, M.; Paolucci, F.; Roffia, S.; Alebbi, M.; Bignozzi, C. A. *J. Phys. Chem. B* **2002**, *106*, 3926–3932.
(69) Wolfbauer, G.; Bond, A. M.; MacFarlane, D. R. *Inorg. Chem.* **1999**, *38*, 3836–3846.
(70) Zabri, H.; Gillaizeau, I.; Bignozzi, C. A.; Caramori, S.; Charlot, M.-F.; Cano-Boquera, J.; Odobel, F. *Inorg. Chem.* **2003**, *42*, 6655–6666.
(71) Karki, L.; Hupp, J. T. *Inorg. Chem.* **1997**, *36*, 3318–3321.
(72) Vance, F. W.; Hupp, J. T. *J. Am. Chem. Soc.* **1999**, *121*, 4047–4053.

(73) Hug, S. J.; Boxer, S. G. *Inorg. Chim. Acta* **1996**, *242*, 323–327.
(74) Riesen, H.; Krausz, E. *Chem. Phys. Lett.* **1996**, *260*, 130–135.
(75) Riesen, H.; Rae, A. D.; Krausz, E. *J. Lumin.* **1994**, *62*, 123–137.
(76) Riesen, H.; Krausz, E. *Chem. Phys. Lett.* **1993**, *212*, 347–352.
(77) Riesen, H.; Wallace, L.; Krausz, E. *J. Chem. Phys.* **1995**, *102*, 4823–4831.
(78) Riesen, H.; Wallace, L.; Krausz, E. *Int. Rev. Phys. Chem.* **1997**, *16*, 291–359.
(79) Hol, W. G. J. *Prog. Biophys. Mol. Biol.* **1985**, *45*, 149–195.
(80) Lockhart, D. J.; Kim, P. S. *Science* **1993**, *260*, 198–202.
(81) Galoppini, E.; Fox, M. A. *J. Am. Chem. Soc.* **1996**, *118*, 2299–2300.
(82) Booth, F. *J. Chem. Phys.* **1951**, *19*, 391–394.
(83) Booth, F. *J. Chem. Phys.* **1951**, *19*, 1327–1328.
(84) Booth, F. *J. Chem. Phys.* **1951**, *19*, 1615.
(85) Conway, B. E.; Bockris, J. O. M.; Ammar, I. A. *Trans. Faraday Soc.* **1951**, *47*, 756–766.
(86) Bockris, J. O. M.; Habib, M. A. *J. Res. Inst. Catal., Hokkaido Univ.* **1975**, *23*, 47–78.
(87) Grahame, D. C. *Chem. Rev.* **1947**, *41*, 441–501.

JP102349M